Nanostructures of organic molecules and proteins on surfaces

Nabil A. Amro,[a] Jayne C. Garno,[a,b] Maozi Liu,[a] Kapila Wadu-Mesthrige, [b] Gang-yu Liu,*[a]
[a] Department of Chemistry, University of California, Davis, California 95616
[b] Department of Chemistry, Wayne State University, Detroit, Michigan 48202

ABSTRACT

Patterning bioreceptors on surfaces is a key step in the fabrication of biosensors and biochips. State-of-the art technology can produce micrometer-sized biostructures, however, further miniaturization at the nanoscale will require new methods and lithographic tools. In this proceeding, we report three approaches: nanopen reader and writer (NPRW), nanografting and latex particle lithography; for creating nanostructures of small molecules, DNA and proteins. Using nanografting and NPRW, nanostructures of thiol molecules or thiolated ssDNA are fabricated within self-assembled monolayers. Proteins attach selectively to nanopatterns of thiol molecules containing bioadhesive groups such as aldehyde or carboxylates. Using latex particle lithography, arrays of protein nanostructures are produced with high throughput on mica and gold substrates. Near-physiological conditions are used in structural characterization, thus the orientation, reactivity and stability of proteins and DNA molecules within nanostructures may be monitored directly via AFM. While AFM-based approaches provide the highest precision, nanoparticle lithography can produce arrays of protein nanostructures with high throughput. The nanostructures of proteins produced by these approaches provide an excellent opportunity for fundamental investigations of biochemical reactions on surfaces, such as antigen-antibody recognition and DNA-protein interactions. These methods provide a foundation for advancing biotechnology towards the nanoscale.

Keywords: nanopatterns, nanografting, NPRW, nanostructures of proteins, DNA nanopattern, nanolithography, nanofabrication, particle lithography, BSA, IgG

1. INTRODUCTION

Micropatterns of bioreceptors such as DNA, proteins, and oligonucleotides have revolutionized the life science and biomedical industries.[1] Microfabricated DNA chips or DNA microarrays have been used to measure the expression levels of genes in plant, yeast, and human samples.[2-4] DNA or protein microarrays have also been used in disease diagnosis.[5-7] Microarrays of peptides using fluorescent probes are also used to screen large numbers of compounds produced by combinatorial chemistry for potential drugs in the pharmaceutical industry.[8] Further miniaturization of these bioarrays or biochips offers the rewards of reduced quantities of analytes and reagents, increased density of sensor and chip elements, and faster reaction/response time.[9-13] More importantly, by nanofabrication of bioreceptors, one may be able to influence or control bioreactions, since the dimensions of bioentities such as proteins are on the order of nanometers. One prospective application is to regulate cell extracellular matrix protein interactions by positioning these proteins on surfaces with nanometer precision.

Micropatterns can be readily produced using well-known techniques, including photolithography,[12,14-17] and micromachining.[18] These techniques typically fabricate features as small as 1 μm. Recent advances in electron and argon ion beam lithography and microcontact printing[17,19-23] have broken the wavelength barrier to produce patterns as small as 300 nm.[18,24-26] To generate patterns smaller than 100 nm requires new strategies, both for fabrication and characterization.

Scanning probe microcopy methods, such as scanning tunneling microscopy (STM)[27] and atomic force microscopy (AFM)[28] are well known for their unprecedented spatial resolution.[29-32] Taking advantage of the sharpness of the tips, and strong and localized tip-surface interactions, scanning probe microscopy has also been used to manipulate atoms on metal surfaces, and to fabricate nanopatterns of metal and semiconductor surfaces.[33-39] Various approaches for controlling the local interactions between the tip and surface molecules have also been reported. These methods include

Physical Chemistry of Interfaces and Nanomaterials, Jin Z. Zhang, Zhong L. Wang, Editors, Proceedings of SPIE Vol. 4807 (2002) © 2002 SPIE · 0277-786X/02/$15.00

AFM-based lithography such as tip-catalyzed surface reactions,[40] dip-pen nanolithography,[41] tip-directed formation of metal-oxide devices,[42,43] and STM-based lithography such as tip-assisted electrochemical etching, and field-induced desorption.[44,45]

In this proceeding, we report the utilization of AFM-based lithographic methods, nanografting and NPRW, as well as nanoparticle lithography in production of nanostructures of proteins and DNA. The advantage of these approaches is the high spatial precision. One shortcoming of scanning probe lithography is the relatively low throughput. Complementary to AFM-based lithography, nanoparticle or nanosphere lithography has high throughput. Arrays of nanostructures of proteins may be produced via nanoparticle lithography.

2. MATERIALS AND METHODS

2.1 Preparation of self-assembled monolayers

The compounds 2-mercapto-1-propionic acid ($HS(CH_2)COOH$, 1-hexanethiol ($HS(CH_2)_5CH_3$), 1-decanethiol, ($HS(CH2)_9CH_3$), and 1-octadecanethiol ($HS(CH_2)_{17}CH_3$) were purchased from Aldrich (St. Louis, MO) with purity greater than 95%. Compounds of 3-mercapto-1-propanal ($HS(CH_2)_2CHO$), and 11-mercapto-1-undecanal ($HS(CH_2)_{10}CHO$), were synthesized by oxidizing with pyridium dichromate (PDC).[46] Ultraflat gold films, 150 nm in thickness, were prepared according to previously reported methods.[47,48] The resulting gold surfaces have a mean roughness of 2–5 Å according to AFM measurements. SAMs were prepared by immersing freshly prepared gold films into corresponding thiol solutions (0.1 to 1.0 mM) for at least 18 h.

2.2 Solutions of proteins and latex particles

Bovine serum albumin (BSA, fraction V, which is essentially fatty acid free), lysozyme (LYZ, from hen egg, 95% purity), rabbit immunoglobulin G (IgG, purity 95%), and mouse anti-rabbit IgG were purchased from Sigma Biochemicals (St. Louis, MO) and used without further purification. The proteins were diluted to the desired concentrations of 10 μg/mL in HEPES or PBS buffer solutions prior to AFM experiments.

Latex particles were obtained commercially (Duke Scientific, Palo Alto, CA). The latex particles were washed in deionized water by centrifugation. The latex pellets were resuspended with deionized water and vortex mixing. Protein concentrations ranged from 10-200 μg/mL and were added to the latex solution according to the desired protein:latex ratio.

2.3 Oligonucleotides

The thiolated ssDNA oligomers used for fabrication were 5'-HS-$(CH_2)_6$CTAGCTCTAATCTGCTAG-3' (oligo 1), and 5'-HS-$(CH_2)_6$AGAAGGCCTAGA-3' (oligo 2) (Synthegen LLC, TX).

2.4 Optical microscopy.

Optical micrographs were acquired using an Olympus model BH-2 phase contrast microscope. Digital images were acquired with a Sony DXC-107 color video CCD camera, with a 768 x 494 pixel chip. The computer interface includes an Osprey 100 video capture card and its driver (version 1.2.00), using the VidCap 32 software within Windows98. Samples were immersed in Cargill type DF immersion oil (Electron Microscopy Sciences, Washington, PA) for examination under 100× objective. The video-capture images were further magnified for the CCD camera using a 2.5× objective.

2.5 Atomic force microscopy

The AFM used for this study incorporates a home-constructed, deflection type scanner controlled by commercial electronics and software (RHK Technology, Inc., Troy, MI).[49,50] The Si_3N_4 cantilevers were either sharpened microlevers from ThermoMicroscopes (Sunnyvale, CA) with a force constant of 0.1 N/m or standard microlevers from Digital Instruments (Santa Barbara, CA) with a force constant of 0.38 N/m. Images were acquired with a typical imaging force of 0.15 nN using contact mode imaging in liquid media, where little tip-induced deformation was observed for immobilized proteins.

3. RESULTS AND DISCUSSION

3.1 Basic procedures to fabricate nanometer-sized patterns

Figure 1 illustrates the basic procedures of nanografting and NPRW used to produce nanopatterns of SAMs with high precision.[51-53] Prior to fabrication, the surface structure of SAM resists are first characterized under a very low force or load. Fabrication locations are selected, typically in flat regions, e.g. Au(111) plateau areas with few surface defects. Then nanopatterns are fabricated under high forces. In nanografting,[54] the SAM and the cantilever are immersed in a solution containing another thiol with various terminal groups (Fig. 1A). As the AFM tip plows through the matrix under high force, thiol molecules on surface are shaved to expose areas of the gold surface (Fig. 1B). Thiols in solution immediately adsorb to the uncovered substrate, following the scanning trajectory of the tip. Returning to low force, the nanografted patterns can be characterized (Fig. 1C). In NPRW, the tip is coated with desired molecules by soaking in the desired solution, then drying in nitrogen. The first step is reading or characterization, in which the matrix SAM is characterized and areas for fabrication are selected. The second step is writing or fabrication, in which the molecules from the tip are transferred under high force to the substrate (Fig. 1E). Nanostructures are characterized in the final step using the same pen at a reduced force (Fig. 1F).[52] Nanopatterns of protein-adhesive thiol molecules produced by nanografting and NPRW can serve as templates for attaching proteins. The selectivity of protein adsorption is achieved by utilizing the variation in protein affinity towards different SAMs.[55-59]

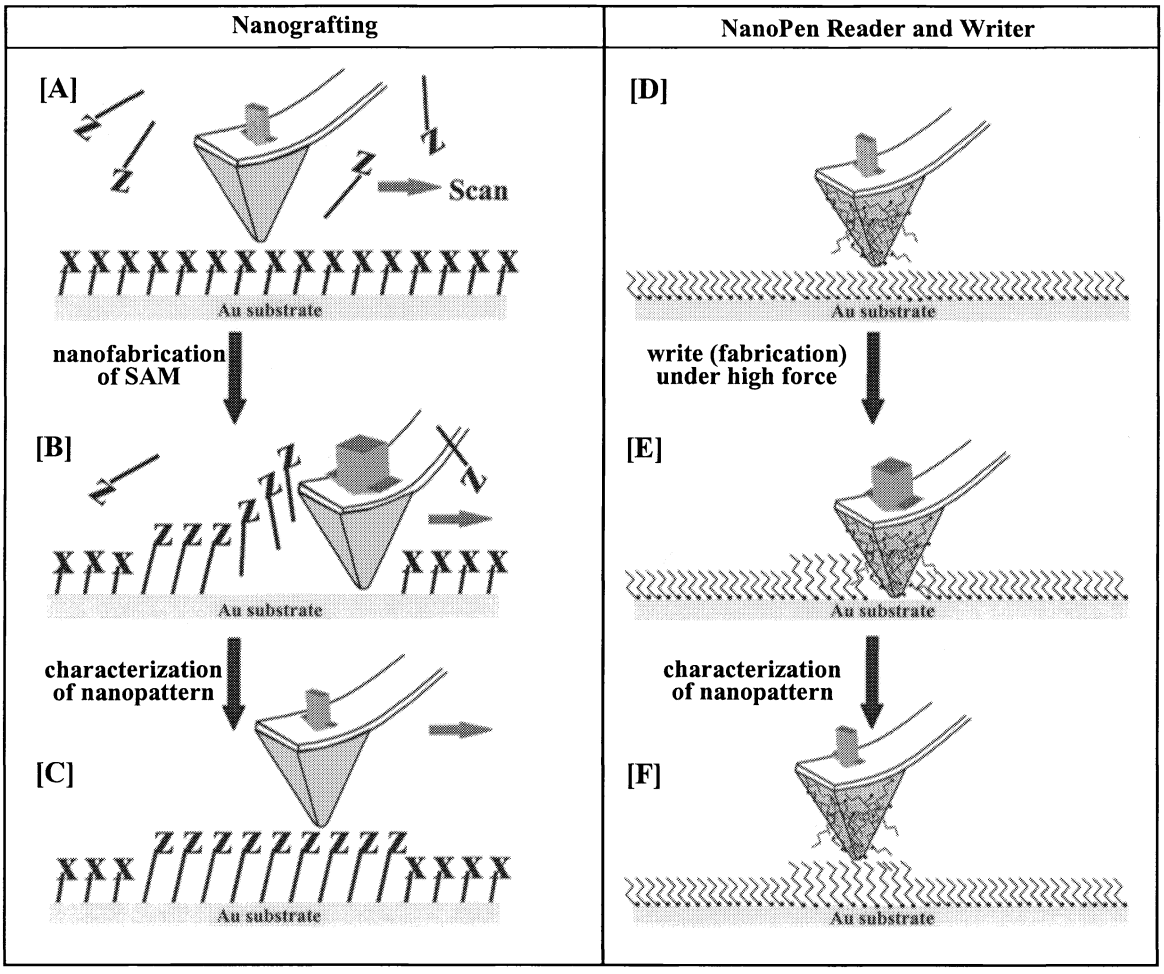

Figure 1. Schematic diagram illustrating the basic steps of nanografting and NanoPen Reader and Writer (NPRW)

Compared to other fabrication techniques, nanografting and NPRW have the highest precision and resolution, and can routinely obtain an edge resolution of 1 nm.[50,52] The smallest feature fabricated by nanografting is 2 x 4 nm^2, as shown in Fig. 2A, consisting of 32 thiol molecules.[53] One-dimensional features such as 10 nm wide lines (Fig. 2B),[52] or two-dimensional nanoislands with various shapes can also be engineered. More importantly, for positioning biomolecular building blocks, bioadhesive ligands such as biotin, -COOH, and –CHO can be positioned with nanometer precision.[60] In Fig. 2C, an $HS(CH_2)_{17}CH_3$ pattern (600 x 600 nm^2) was first grafted within an $HS(CH_2)_9CH_3$ matrix, to produce a nanosquare of positive contrast. Then, two nanostructures of aldehyde-terminated thiols, a 70 x 70 nm^2 square and a 70 x 300^2 nm rectangle were produced within the $HS(CH_2)_{17}CH_3$ nanosquare.

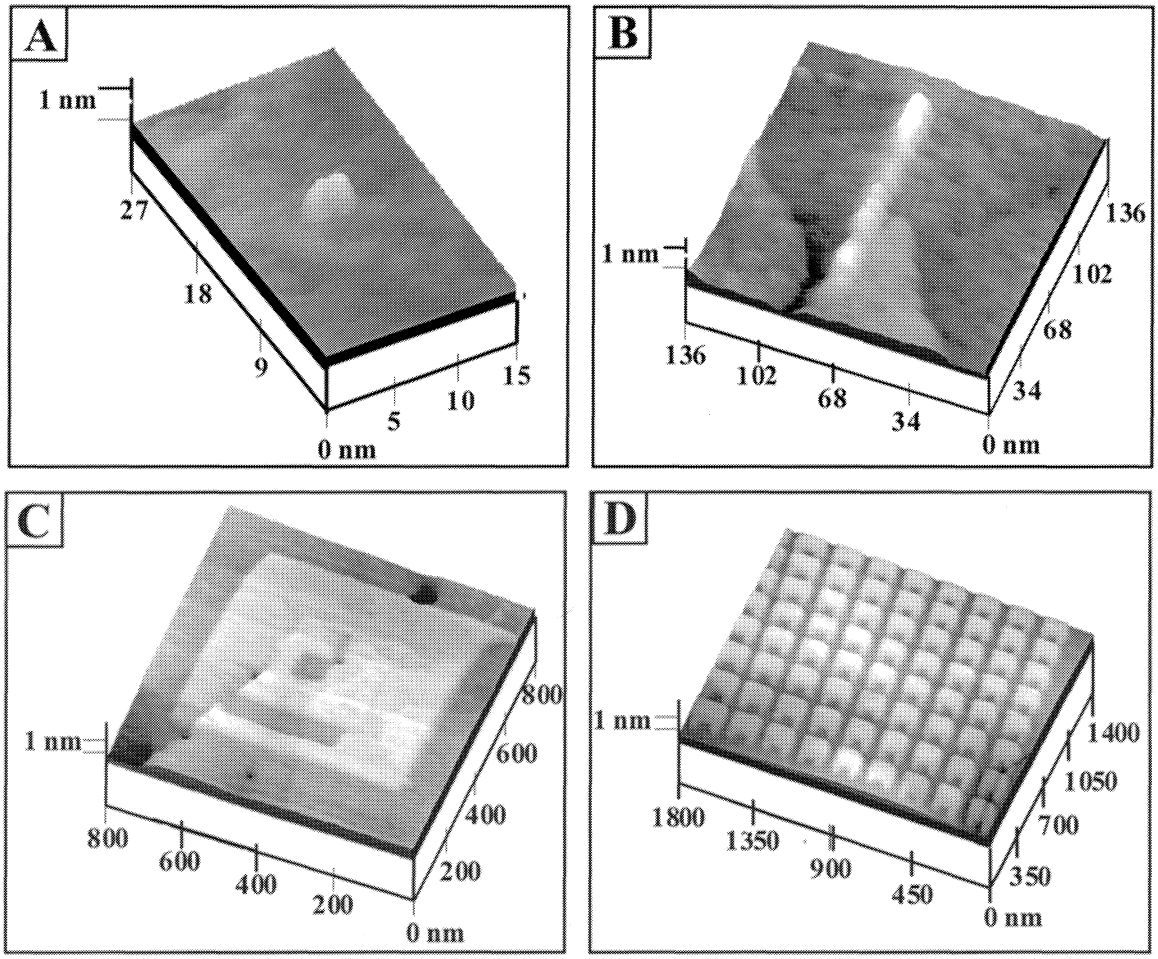

Figure 2. Nanopatterns produced within a $CH_3(CH_2)_9S$/Au(111) monolayer using AFM-based lithography. (A) Thirty-two $CH_3(CH_2)_{17}SH$ molecules are grafted to form a 2 x 4 nm^2 "dot." The "dot" is 8.8 Å higher than the surrounding monolayer, indicating that thiols are closely-packed. (B) A 10 x 100 nm^2 line of $CF_3(CF_2)_{11}(CH_2)_2SH$ molecules produced using NPRW. (C) Nanostructures with multiple components may be produced. Two small patterns of aldehyde-terminated SAMs are grafted into a 600 x 600 nm^2 square area of $CH_3(CH_2)_{17}SH$. (D) Fabrication of arrays of nanostructures. Each element consists of $CH_3(CH_2)_{17}SH$ molecules. This array was fabricated in four minutes using automated scanning probe lithography.

The example shown in Fig. 2C demonstrates the capability of nanografting for producing nanostructures with various heights and functionalities. The proof-of-concept experiment in Fig. 2D displays a 9 x 8 array of nanostructures. Each element has a 150 x 115 nm^2 head attached to two small "legs" of 40 x 45 nm^2. The nanostructures consist of octadecanethiol, which is 0.8 nm taller than the decanethiol matrix. The examples in Fig. 2 demonstrate the precision of AFM-based lithography for positioning small molecules, as well as the flexibility in designing nanostructures with

various shapes, size and reactivities.[61] The nanostructures of these ligands are not observed to exhibit lateral diffusion, due to their organization into closely packed structures which are surrounded by matrix SAMs.

3.2 Production of protein nanopatterns

The success of our approach relies upon production of nanometer-sized patterns of SAMs, and on the selective adsorption of proteins onto these patterns. The quality of the protein nanostructures depends on the spatial precision of nanopatterns and on the selectivity of protein adsorption. In Fig. 3, lysozyme (LYZ) nanopatterns were produced via electrostatic immobilization. The two patterns, a narrow line (10×150 nm^2) above a rectangle (100×150 nm^2), were fabricated into the decanethiol matrix. The two patterns are separated by 30 ± 5 nm as shown in Fig. 3A. Both patterns exhibit negative contrast in the topographic image because the chain length of mercapto-propanoic acid is 0.5 ± 0.1 nm shorter than the matrix thiols. Prior to protein adsorption, the patterned SAM was washed with deionized water and then

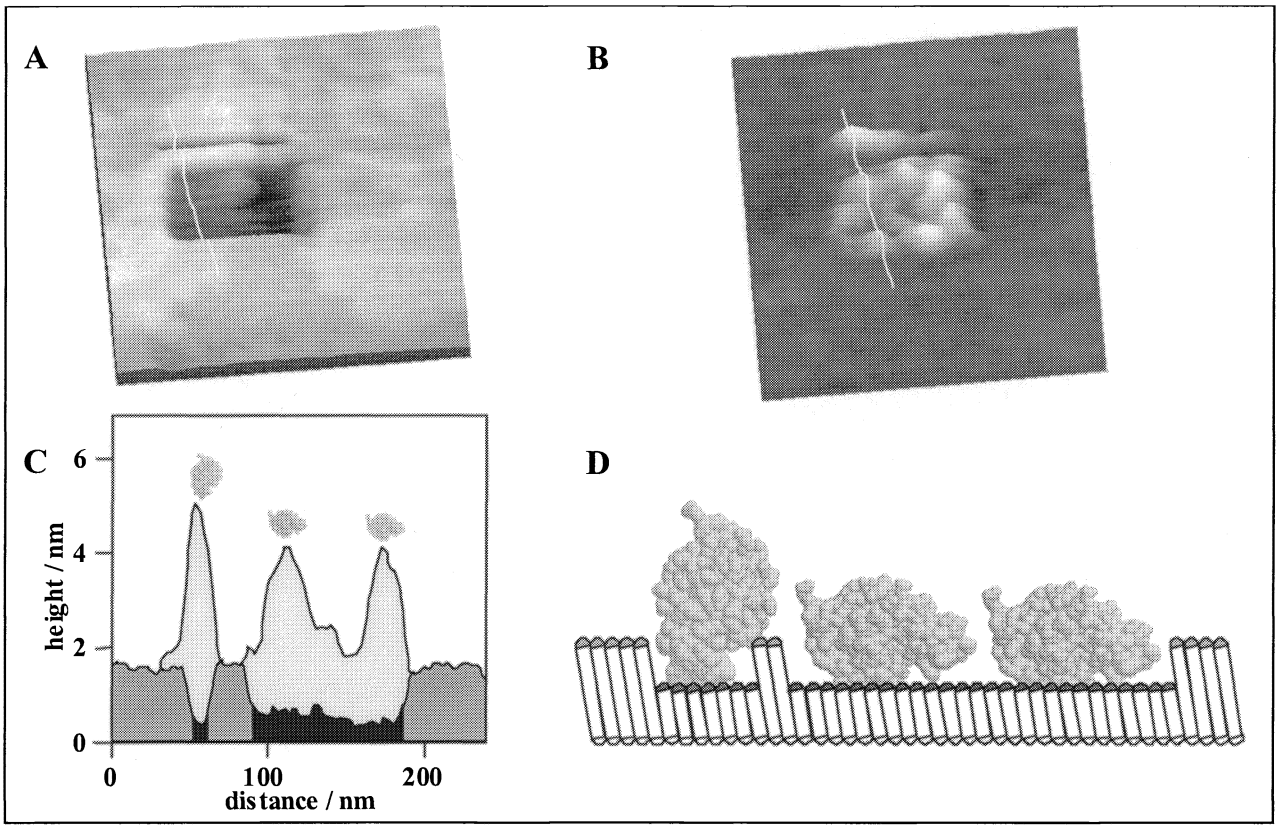

Figure 3. Nanopatterns of LYZ produced by immobilization of proteins via electrostatic interactions. (A) A 10×150 nm^2 line and a 100×150 nm^2 rectangle of 3-mercapto-1-propanoic acid nanografted within a 400×400 nm^2 area of a decanethiol SAM; (B)The same area imaged after 4-min incubation with a LYZ solution. (C) Corresponding cursor profile of the protein nanopatterns. The origin of the Y-axis is the gold surface. The cursor profile of the corresponding patterned SAM is shown in the same plot. The dark gray, solid filled area represents undisturbed matrix SAM, the area filled black follows the topography of the nanografted pattern from the white lines in image B, the light gray areas show the adsorbed protein, for the cursor line in B. (D) Schematic diagram depicts the orientation of protein upon adsorption.

with 20 mM HEPES buffer (pH 7.0) to remove any remaining thiol molecules. After rinsing, a 10 μg/ml solution of LYZ was injected into the AFM liquid cell. Within 3 min, proteins adsorbed exclusively onto the two patterned areas, as shown in Fig. 3B. The high selectivity observed at pH 7 is mostly due to electrostatic attraction between the LYZ molecules and the carboxylate-terminated nanopatterns. Because the IEP of LYZ is 11.1,[62] LYZ exhibits a net positive charge at pH 7. The pKa value of mercapto-propanoic acid SAM is 8,[63] thus at neutral pH, ~10% of the nanopatterned area has a net negative charge. Therefore, electrostatic attractions drive the selective adsorption of LYZ onto the carboxylic-terminated areas instead of the methyl-terminated area. Under these conditions, little adsorption was observed

at methyl-terminated areas within the time frame of the entire experiment (4 h). Furthermore, the boundary between the two nanopatterns remained clearly visible. Individual LYZ particles within the patterns can be clearly resolved in the AFM image of Fig. 3B. The corresponding cursor profiles in Fig. 3C reveal that the immobilized protein molecules exhibit two different heights: 4.3 ± 0.2 nm and 3.0 ± 0.2 nm. It is known that physical interactions are not specific; therefore, various orientations with respect to the surface are observed for the adsorbed proteins. Because LYZ molecules are ellipsoidal with the approximate dimensions 4.5 × 3.0 × 3.0 nm^3 from X-ray crystallographic studies,[64] the observed heights correspond to side-on and end-on orientations of LYZ, presented in the schematic diagram (Fig. 3D).

3.3 Reactivity and stability of protein nanostructures

We tested the reactivity and stability of nanopatterns of proteins. Figure 4 shows an example in which the bioactivity of nanostructures of rabbit IgG was tested by adding specific antibody, mouse anti-rabbit IgG. In Fig. 4A,

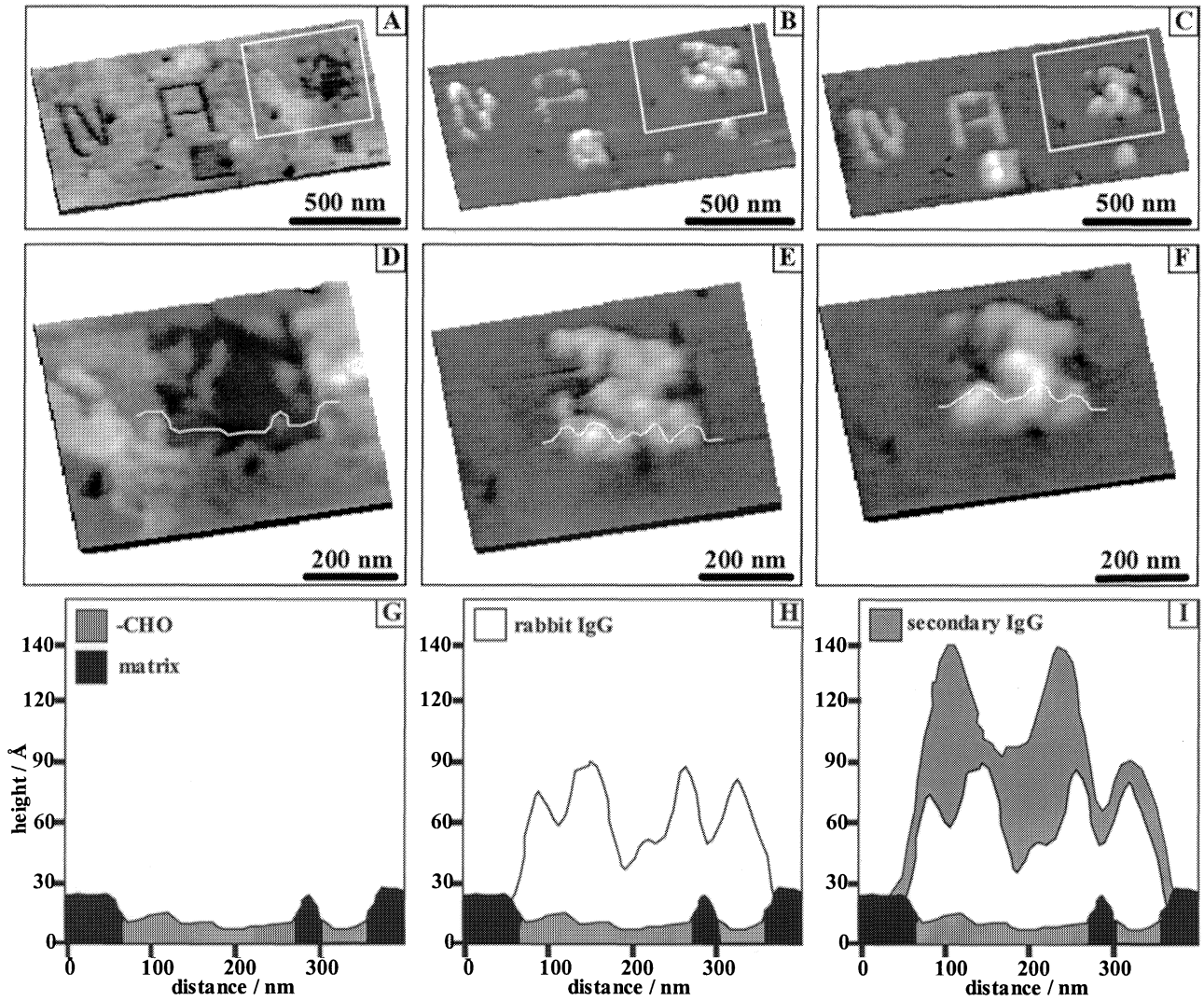

Figure 4. Recognition (binding) of rabbit IgG within nanopatterns by specific mouse-anti-rabbit IgG. (A) Nanopatterns of mercapto-undecanal: 250 x 250 nm^2, 100 x 100 nm^2, and a linewidth of 25 nm for the two letters. An incomplete pattern 300 x 300 nm^2 on the right was formed by using a smaller fabrication force. (B) The same area after immersing in a 0.01 mg/ml solution of rabbit IgG for 3 min followed by washing. (C) After introducing mouse anti-rabbit IgG, the patterns display an increase in height, indicating the specific binding of antibody to the immobilized protein. (D-F) Higher-resolution topographic images were acquired by zooming into the areas indicted in (A-C). (G–I) Corresponding cursor profiles following the fabrication and recognition process.

several aldehyde-terminated patterns, were first grafted. Three squares with sizes 250 x 250 nm^2, 100 x 100 nm^2, and 300 x 300 nm^2 are shown. The third pattern, (upper right corner) contains mixed dodecanethiol and mercaptoundecanal, resulting from incomplete removal of the matrix SAM during nanografting. Two letters "N" and "A" were also produced, which have a linewidth of 25 nm. Gold steps and defects are clearly visible throughout the experiments. The depth of these negative-height patterns is 6.0 ± 1.0 Å, in good agreement with the expected height difference between the SAM and the patterns. After the templates were created, the liquid cell was washed with water and PBS buffer. Rabbit IgG was injected, and adsorption was observed on all five patterns. The covalent immobilization of rabbit IgG on aldehyde-terminated nanopatterns is highly stable. Washing with 1% Tween 20 and PBS did not change the pattern. During the 36 hr experimental period, no morphology changes of the protein patterns were observed. There is a clear increase in height, after injecting protein solution and rinsing, as demonstrated in the AFM topographs of Figs. 4A and 4B. With IgG bound to the nanopatterns, the heights range from 3.0 - 4.4 nm taller than the octadecanethiol matrix. Analysis of the entire set of patterns indicates that IgG molecules exhibit heights ranging from 3.8 to 7.0 nm. The variation in height is consistent with the expectation that each rabbit IgG has 57 lysine residues containing amines (PDB ID code 1IGT). Thus immobilized IgG may adopt various configurations after reacting with aldehyde.

Specific recognition of the fabricated antigenic address to anti-rabbit IgG is demonstrated in Fig. 4C. Rabbit IgG in solution was removed from the AFM liquid cell before injecting secondary antibodies. Figure 4C shows the same region of the surface presented in Figs. 4A and 4B, after 10 min of exposure to mouse anti-rabbit IgG. A further increase in height was observed after the injection, ranging from 2.8 to 7.5 nm, indicating the attachment of the secondary antibody. A wide height range is expected because the rabbit IgG molecules within the patterns have various orientations on surfaces. Higher-resolution topographic images are shown for the mixed SAM nanopattern within the white frame (Figs. 4D-4F). The heights of the nanopatterns are more quantitatively illustrated from the cursor profiles in Figs. 4G-4I. The end of the F_c fragment of each rabbit IgG serves as the binding site for the mouse anti-rabbit IgG. The ends of the F_{ab} fragment of the Y-shaped mouse anti-rabbit IgG bind specifically to the rabbit IgG. Various orientations of the rabbit IgG lead to different configurations of the antibody-antigen binding complexes. In contrast, injection of non-specific antibodies did not result in any observable height increase.

3.4 Nanostructures of thiolated single-stranded DNA

Nanostructures of single-stranded DNA (ssDNA) can be produced using nanografting. Fig. 5A shows a 115 × 135 nm^2 nanopattern of oligo 1 (18-nucleotide ssDNA) grafted within a $CH_3(CH_2)_5S$/Au(111) matrix. Nanografting and imaging of the DNA patterns were conducted in a liquid medium containing 40 μM ssDNA. The fabrication was accomplished using a force of 20 nN and at a speed of 800 nm/s. The cursor profile in Fig. 5D indicates that the oligo 1 pattern measures 54 - 74 Å higher than the matrix SAM (or 63 - 83 Å of the total length). Figure 5B reveals another example, in which a 190 × 230 nm^2 pattern of oligo 2 (12 - nucleotide ssDNA) was grafted into a different alkanethiol matrix, $CH_3(CH_2)_9S$/Au(111). The height difference between the pattern and matrix measured 36 - 46 Å, as shown in the corresponding cursor profile in Fig. 5E. Thus, the oligo 2 molecules have total heights ranging from 50 to 60 Å. In Fig. 5C, three ssDNA nanolines of oligo 2, were grafted by a single scan. The sizes of a_1-a_3 are 20 × 170 nm^2, 15 × 150 nm^2, 25 × 160 nm^2, respectively. The matrix is decanethiol SAM. The narrowest width of the DNA line patterns we have achieved is 10 nm. The apparent heights are shown in the cursor profile (Fig. 5F). The overall height appears lower than the rectangular pattern because the lines are subject to tip pressure. The middle pattern, a2, is a broken line, in which the smallest ssDNA dot is 7 × 11.5 nm^2 (indicated by an arrow). Assuming that DNA forms a close-packed structure and the cross section diameter of ssDNA is 20 Å, this dot consists of only 26 molecules.

The measured DNA heights within the nanopattern correspond well with a standing-up and nearly stretched configuration. The variation in DNA height within the pattern is likely due to variations in configuration. Achieving a standing-up orientation is very important for the performance of the DNA patterns, particularly when used as sensing elements. The accessibility of a DNA pattern with molecules lying down will be hindered by the substrate, and thus the performance of such an array is likely to be compromised. The fabrication method described here provides a promising way to make DNA arrays in which the orientation and position of DNA molecules can be well controlled.

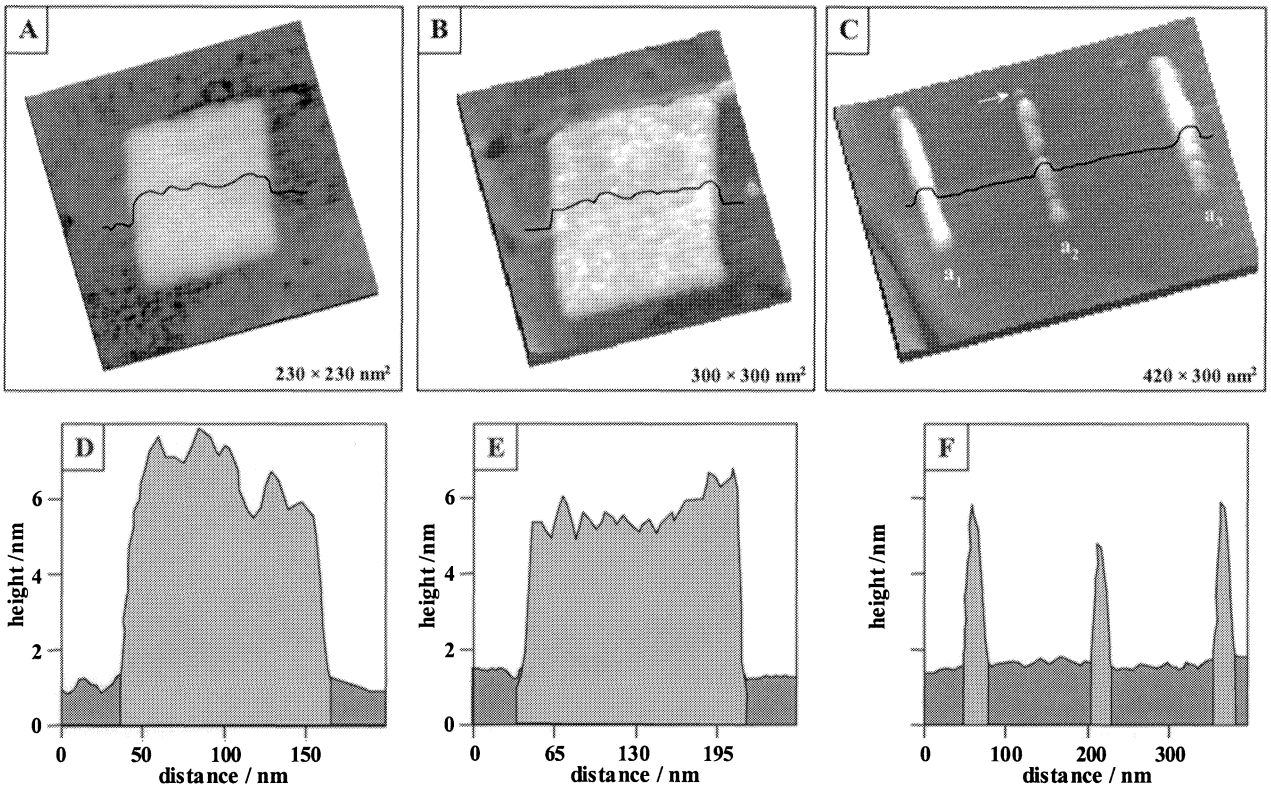

Figure 5. Positioning ssDNA on gold surface. (A) A 115 × 135 nm^2 square of oligo 1 nanostructure grafted within a hexanethiol SAM. (B) A 190 × 230 nm^2 rectangle of oligo 2 fabricated within a decanethiol SAM. (C) Three nanolines of oligo 2 with sizes 20 × 170 nm^2, 15 × 150 nm^2, 25 × 160 nm^2 were produced within a decanethiol SAM: a1 and a3 are solid lines, while a2 is a broken line. (D-F) Corresponding cursor profile for images (A-C).

3.5 Periodic Arrays of BSA Nanostructures on Mica

Complementary to nanografting and NPRW, we have developed a new method, latex particle lithography, to produce periodic arrays of protein nanostructures with high throughput. The procedure is illustrated in Fig. 6. First the protein and latex are mixed together in an aqueous solution (Fig. 6A). For best results, the solution containing protein and latex is allowed to remain at room temperature for time intervals ranging from 10 min to 4 hours.

In the second step, (Fig. 6B), the colloidal suspension is deposited on the substrate and then allowed to dry. As it dries, the protein and latex mixture adsorbs to mica to form ordered assemblies. Next, the latex is rinsed away with deionized water to produce periodic arrays of protein nanostructures on the substrate, shown schematically in Fig. 6D. The assembly of latex particles and the protein nanostructures can be characterized using AFM at various stages of the nanofabrication process.

In order for this protocol to succeed, the protein needs to exhibit strong adhesion, whereas latex needs to adhere weakly to the substrate. Further, the adhesion between the protein and latex needs to be relatively weak, in order for the latex to be released by rinsing. Polystyrene latex spheres have relatively weak adhesion to hydrophilic mica in comparison to the proteins, and thus can be selectively removed. Another requirement is for the substrate to be flat, to minimize defect formation during the assembly of latex spheres.

The long-range order and periodicity of the 2D array is maintained after removal of the latex template. Figure 7A is an optical microscopy image of BSA arrays immediately after removal of the latex template, 802 ± 6 nm in diameter. The morphology spans the entire mica substrate, typically 1 cm^2 in surface area. Figure 7A also demonstrates the high throughput nature of particle lithography. For latex particles smaller than 800 nm, AFM was employed for imaging because it has higher resolution than optical microscopes. Figure 7B shows an AFM topograph of a BSA array formed after removing a template of 503 ± 4 nm latex particles. At a BSA:latex ratio of 61,000:1, particle lithography yields a BSA array with a periodicity measuring 556 ± 65 nm.

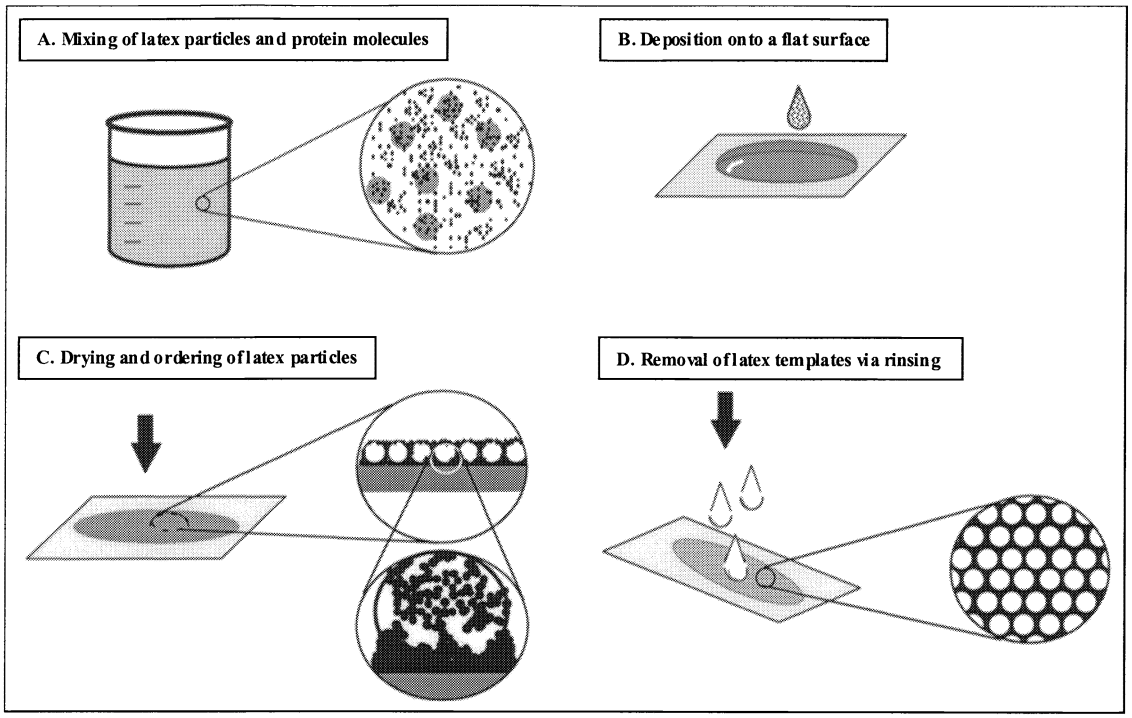

Figure 6. Schematic diagram of the basic procedure to produce protein nanostructures using particle lithography.

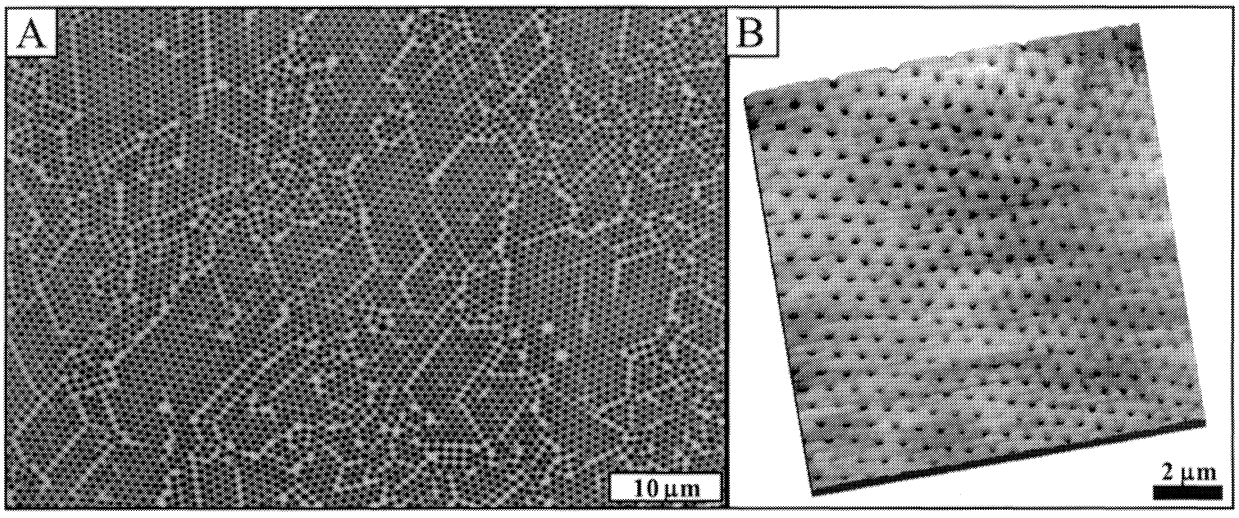

Figure 7. (A) Optical micrograph (65 x 45 μm^2) of a 2-D BSA array on mica(0001) immediately after removal of latex (802 ± 6 nm). The BSA:latex ratio is 398,000:1. The micrograph displays broad regions of periodic dots, spanning 5 to 40 μm^2 areas. The removal of latex was not complete in this example, as identified by the white opaque contrast in the images. (B) AFM topograph for a 12 x 12 μm^2 area of an array of BSA nanostructures produced after 503 nm latex were rinsed away. The BSA:latex ratio is 61,000:1.

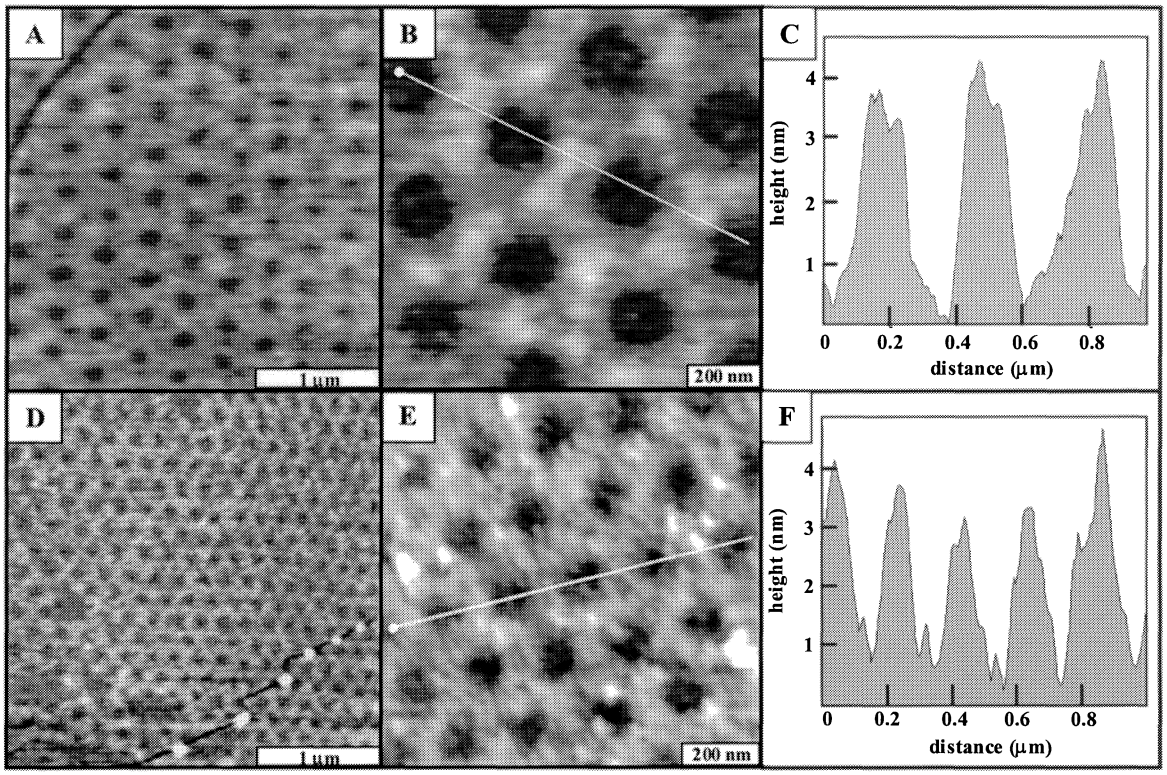

Figure 8. Periodic arrays of BSA nanostructures produced by particle lithography. (A) AFM topograph of a 3 x 3 μm^2 area of a BSA pattern after the 304 nm latex were removed, acquired using CRI[65] at 37.6 kHz and 204 mV. The BSA:latex ratio is 9,000:1. (B) High-resolution view of a 1 x 1 μm^2 area of A. (C) Cursor profile for the line in B, shows a height of 3.9 ± 0.3 nm. (D) Topograph of a 3 x 3 μm^2 area for a BSA pattern from 204 nm latex, acquired in ethanol using CRI at 29.3 kHz and 408 mV. The BSA:latex ratio is 9,000:1. (E) Topograph for a 1 x 1 μm^2 scan area. (F) Cursor profile for the line in E, indicates a height of 3.8 ± 0.5 nm.

Arrays of BSA nanostructures with even smaller periodicity can be produced. Using 304 ± 5 nm diameter latex particles as templates, the resulting BSA nanostructures are shown in Figs. 8A and 8B. The periodicity in this example is 335 ± 37 nm. The thickness of the protein nanostructures measured from the corresponding cursor in Fig. 8C is 3.9 ± 0.3 nm, corresponding well with the diameter of BSA (4.0 nm).[66]

Nanoparticle lithography also works with latex spheres as small as 204 nm, (Figs. 8D-F). The cursor in Fig. 8F shows a height of 3.8 ± 0.5 nm. The periodicity measured 189 ± 24 nm. The arrays of BSA nanostructures are stable under ambient conditions. In buffer solution, the stability was tested by imaging a sample immersed in PBS buffer over time. The pattern remained unchanged for the 16 hr duration of the experiment.

The detailed morphology and periodicity of protein nanostructures are determined by the latex diameter and protein:particle ratio. Typically, the heights of protein nanostructures correspond to the dimensions of single protein molecules. Our method of latex particle lithography was also applied to IgG, in which AFM measurements show that antibodies adopt various orientations when adsorbed on surfaces. The arrays were tested to see if the proteins maintain their activity, and the proteins within the nanostructures retain the ability to bind corresponding specific antibodies.

4. CONCLUSIONS

We have reported three approaches for nanolithography using small molecules, DNA and proteins: nanografting, NPRW and nanoparticle lithography. AFM-based lithography, such as nanografting and NPRW, achieve the highest spatial resolution. Using these methods, nanostructures of thiol molecules have been produced successfully with various

chain lengths and terminal groups such as –OH, $-CO_2H$, $-NH_2$, and –CHO.[60,61] Nanoislands of only 32 alkanethiol molecules were produced on metal surfaces.[51] Individual proteins can be aligned on a 10×150 nm^2 line.[46] Nanopatterns consisting of 26 molecules of ssDNA were positioned within a SAM matrix.[67] Arrays of protein nanostructures were produced on mica and gold surfaces with high throughput.[68] Nanostructures produced via nanografting and NPRW are characterized *in situ* using the same AFM probe. While it is more difficult to position and image protein systems, our approaches allow individual protein molecules be immobilized and imaged. Since near-physiological conditions are used in structural characterization, the orientation, sensitivity and stability of protein and DNA molecules within nanostructures may be directly monitored and measured via AFM. Complementary to AFM lithography, nanoparticle lithography produces arrays of protein nanostructures with high throughput.

Nanostructures produced by these approaches provide an opportunity for investigations of biochemical reactions at interfaces, such as antibody-antigen recognition and DNA-protein interactions. In addition, these methods provide groundwork for future developments in nanotechnology and biotechnology.

5. ACKNOWLEDGEMENTS

This work was supported by the University of California, Davis and NSF (IGERT-970952 and 9972741).

REFERENCES

1. C. Nicolini, "From Neural Chip and Engineered Biomolecules to Bioelectronic Devices - an Overview," *Biosens. Bioelectron.* ***10***, pp. 105-127, 1995.
2. M. Schena, D. Shalon, R. Heller, A. Chai, P. O. Brown, R. W. Davis, "Parrallel Human Genome Analysis: Microarray-Based Expression Monitoring of 1000 Genes," *Proc. Natl. Acad. Sci.* ***93***, pp. 10614, 1996.
3. G. Ramsy, "DNA Chips: State-of-the Art," *Nature Biotechnology* ***18***, pp. 40, 1998.
4. J. Cairney, N. F. Xu, G. S. Pullman, V. T. Ciavatta, B. Johns, "Natural and Somatic Embryo Development in Loblolly Pine Gene Expression Studies Using Differential Display and DNA Arrays," *Appl. Biochem. Biotech.* ***77-9***, pp. 5, 1999.
5. A. S. Blawas, T. F. Oliver, M. C. Pirrung, W. M. Reichert, *Langmuir* ***14***, pp. 4243, 1998.
6. G. Wittstock, B. Grundig, B. Strehlitz, K. Zimmer, "Evaluation of microelectrode arrays for amperometric detection by scanning electrochemical microscopy," *Electroanalysis* ***10***, pp. 526-531, 1998.
7. R. L. Edelstein, C. R. Tamanaha, P. E. Sheehan, M. M. Miller, D. R. Baselt, L. J. Whitman, R. J. Colton, "The BARC biosensor applied to the detection of biological warfare agents," *Biosens. Bioelectron.* ***14***, pp. 805-813, 2000.
8. S. P. A. Fodor, J. Leighton Read, M. C. Pirrung, L. Stryer, A. T. Lu, D. Solas, "Light-Directed, Spatially Addressable Parallel Chemical Synthesis," *Science* ***251***, pp. 767, 1991.
9. J. S. Marvin, E. E. Corcoran, N. A. Hattangadi, J. V. Zhang, S. A. Gere, H. W. Hellinga, *Proc. Natl. Acad. Sci.USA* ***94***, pp. 4366-4371, 1997.
10. P. Bergveld, *Sensors and Actuators A* ***56***, pp. 65-73, 1996.
11. M. Eggers, M. Hogan, R. K. Reich, J. Lamture, D. Ehrlich, M. Hollis, B. Kosicki, T. Powdrill, K. Beattie, S. Smith, R. Varma, R. Gangadharan, A. Mallik, B. Burke, D. Wallace, *BioTechniques* ***17***, pp. 516, 1994.
12. J. C. O'Brien, V. W. Jones, M. D. Porter, *Anal. Chem.* ***72***, pp. 703-710, 2000.
13. R. E. Kunz, *Sensors and Actuators B*, pp. 38-39, 1997.
14. V. W. Jones, J. R. Kenseth, M. D. Porter, *Anal. Chem.* ***70***, pp. 1233-1241, 1998.
15. D. V. Nicolau, T. Taguchi, H. Taniguchi, S. Yoshikawa, "Micron-Sized Protein Patterning on Diazonaphthoquinone/Novolak Thin Polymeric Films," *Langmuir* ***14***, pp. 1927, 1998.
16. N. Dontha, W. B. Nowall, W. G. Kuhr, *Anal. Chem.* ***69***, pp. 2619-2625, 1997.
17. A. Bernard, E. Delamarche, H. Schmid, B. Michel, H. R. Bosshard, H. Biebuyck, "Printing Patterns of Proteins," *Langmuir* ***14***, pp. 2225-2229, 1998.
18. A. A. Bergman, J. Buijs, J. Herbig, D. T. Mathes, J. J. Demarest, C. D. Wilson, C. T. Reimann, R. A. Baragiola, R. Hull, S. O. Oscarsson, "Nanometer-Scale Arrangement of Human Serum Albumin by Adsorption on Defect Arrays Created with a Finely Focused Ion Beam," *Langmuir* ***14***, pp. 6785- 6788, 1998.
19. R. S. Kane, S. Takayama, E. Ostuni, D. E. Ingber, G. M. Whitesides, "Patterning proteins and cells using soft lithography," *Biomaterials* ***20***, pp. 2363-2376, 1999.

20. A. Bernard, J. P. Renault, B. Michel, H. R. Bosshard, E. Delamarche, "Microcontact printing of proteins," *Adv Mater **12***, pp. 1067-1070, 2000.
21. J. Lahiri, E. Ostuni, G. M. Whitesides, "Patterning ligands on reactive SAMs by microcontact printing," *Langmuir **15***, pp. 2055-2060, 1999.
22. T. C. Ta, M. T. McDermott, *Anal. Chem. **72***, pp. 2627-2634, 2000.
23. C. Bieri, O. P. Ernst, S. Heyse, K. P. Hofmann, H. Vogel, *Nature **17***, pp. 1105-1108, 1999.
24. R. C. Tiberio, H. G. Craighead, M. Lercel, T. Lau, C. W. Sheen, D. L. Allara, "Self-assembled Monolayers Electron-beam Resist on GaAs," *Appl. Phys. Lett. **62***, pp. 476-478, 1993.
25. J. A. M. Sondag-Huethorst, H. R. J. Van Helleputte, L. G. J. Fokkink, "Generation of Eelectrochemically Deposited Metal Patterns Means of Electron-Beam (nano) Lithography of Self-Assembled Monolayer Resists," *Appl. Phys. Lett. **64***, pp. 285, 1994.
26. M. Mrksich, C. S. Chen, Y. N. Xia, L. E. Dike, D. E. Ingber, G. M. Whitesides, "Controlling cell attachment on contoured surfaces with self-assembled monolayers of alkanethiolates on gold," *Proc. Natl. Acad. Sci. U. S. A. **93***, pp. 10775-10778, 1996.
27. G. Binnig, H. Rohrer, C. Gerber, E. Weibel, "Surface Studies by Scanning Tunneling Microscopy," *Phys. Rev. Lett. **49***, pp. 57-61, 1982.
28. G. Binnig, C. F. Quate, C. Gerber, "Atomic Force Microscope," *Phys. Rev. Lett. **56***, pp. 930-936, 1986.
29. C. J. Chen, *Introduction to Scanning Tunneling Microscopy*; Oxford University Press, New York, NY, **1993**.
30. D. Sarid, *Scanning Force Microscopy, with Applications to Electric, Magnetic and Atomic Forces*; Oxford University Press: New York, 1991.
31. J. Frommer, "Scanning Tunneling Microscopy and Atomic Force Microscopy Iin Organic-Chemistry," *Angew. Chem. Int. Ltd. Engl. **31***, pp. 1298-1328, 1992.
32. R. J. Hamers, "Scanned Probe Microscopies in Chemistry," *J. Phys. Chem. B **100***, pp. 13103-13120, 1996.
33. D. M. Eigler, E. K. Schweizer, "Positioning Single Atoms with a Scanning Tunneling Microscope," *Nature **244***, pp. 524-526, 1990.
34. P. Zeppenfeld, C. P. Lutz, D. M. Eigler, "Manipulating Atoms and Molecules with a Scanning Tunneling Microscope," *Ultramicroscopy **42-44***, pp. 128-133, 1992.
35. M. F. Crommie, C. P. Lutz, D. M. Eigler, "Confinement of Electrons to Quantum Corrals on a Metal Surface," *Science **262***, pp. 218-220, 1993.
36. T. A. Jung, R. R. Schlittler, J. K. Gimzewski, H. Tang, C. Joachim, "Controlled Room-temperature Positioning of Individual Molecules: Molecule Flexure and Motion," *Science **271***, pp. 181-184, 1996.
37. P. Avouris, "Manipulation of Matter at the Atomic and Molecular Levels," *Acc. Chem. Res. **28***, pp. 95-102, 1995.
38. I. W. Lyo , P. Avouris, "Field-Induced Nanometer-Scale to Atomic-Scale Manipulation of Silicon Surfaces with the STM," *Science **253***, pp. 173-176, 1991.
39. B. C. Stipe, M. A. Bezaei, W. Ho, S. Gao, M. Persson, B. I. Lundqvist, "Single-Molecule Dissociation by Tunneling Electrons," *Phys. Rev. Lett. **78***, pp. 4410-4413, 1997.
40. W. T. Muller, D. L. Klein, T. Lee, J. Clarke, P. L. Mceuen, P. G. Schultz, "A Strategy for the Chemical Synthesis of Nanostructures," *Science **268***, pp. 272-273, 1995.
41. R. D. Piner, J. Zhu, F. Xu, S. H. Hong, C. A. Mirkin, ""Dip-pen" nanolithography," *Science **283***, pp. 661-663, 1999.
42. E. S. Snow, P. M. Campbell, "Afm Fabrication of Sub-10-Nanometer Metal-Oxide Devices with in-Situ Control of Electrical-Properties," *Science **270***, pp. 1639-1641, 1995.
43. J. A. Dagata, T. Inoue, J. Itoh, K. Matsumoto, H. Yokoyama, "Role of space charge in scanned probe oxidation," *J. Appl. Phys. **84***, pp. 6891-6900, 1998.
44. C. B. Ross, L. Sun, R. M. Crooks, "Scanning Probe Lithography .1. Scanning Tunneling Microscope Induced Lithography of Self-Assembled N-Alkanethiol Monolayer Resists," *Langmuir **9***, pp. 632-636, 1993.
45. J. K. Schoer, F. P. Zamborini, R. M. Crooks, "Scanning probe lithography .3. Nanometer-scale electrochemical patterning of Au and organic resists in the absence of intentionally added solvents or electrolytes," *J Phys Chem-Us **100***, pp. 11086-11091, 1996.
46. K. Wadu-Mesthrige, S. Xu, N. A. Amro, G.-Y. Liu, "Fabrication and Imaging of Nanometer-Sized Protein Patterns," *Langmuir **15***, pp. 8580-8583, 1999.

47. M. Hegner, P. Wagner, G. Semenza, "Ultralarge Atomically Flat Template-Stripped Au Surfaces for Scanning Probe Microscopy," *Surf Sci* ***291***, pp. 39-46, 1993.
48. P. Wagner, M. Hegner, H. J. Guntherodt, G. Semenza, "Formation and in-Situ Modification of Monolayers Chemisorbed on Ultraflat Template-Stripped Gold Surfaces," *Langmuir* ***11***, pp. 3867-3875, 1995.
49. W. F. Kolbe, D. F. Ogletree, M. B. Salmeron, "Atomic Force Microscopy Imaging of T4 Bacteriophages on Silicon Substrates," *Ultramicroscopy* ***42***, pp. 1113-1117, 1992.
50. G. Y. Liu, P. Fenter, C. E. D. Chidsey, D. F. Ogletree, P. Eisenberger, M. Salmeron, "An Unexpected Packing of Fluorinated N-Alkane Thiols on Au(111) - a Combined Atomic-Force Microscopy and X-Ray-Diffraction Study," *J Chem Phys* ***101***, pp. 4301-4306, 1994.
51. S. Xu, G. Y. Liu, "Nanometer-Scale fabrication by Simultaneous Nanoshaving and Molecular Self-Assembly," *Langmuir* ***13***, pp. 127-129, 1997.
52. N. A. Amro, S. Xu, G.-Y. Liu, "Patterning Surfaces Using Tip-Directed Displacement and Self-Assembly," *Langmuir* ***16***, pp. 3006-3009, 2000.
53. S. Xu, S. Miller, P. E. Laibinis, G.-Y. Liu, "Fabrication of Nanometer Scale Patterns Within Self-Assembled Monolayers by Nanografting," *Langmuir* ***15***, pp. 7244-7251, 1999.
54. G.-Y. Liu, S. Xu, Y. Qian, "Nanofabrication of Self-Assembled Monolayers Using Scanning Probe Lithography," *Acc. Chem. Res.* ***33***, pp. 457-466, 2000.
55. W. Norde, M. Giesbers, H. Pingsheng, "Langmuir-Blodgett films of polymerized 10,12-pentacosadiyonic acid as substrates for protein adsorption," *Colloid Surface B* ***5***, pp. 255-263, 1995.
56. J. Buijs, D. W. Britt, V. Hlady, "Human growth hormone adsorption kinetics and conformation on self-assembled monolayers," *Langmuir* ***14***, pp. 335-341, 1998.
57. P. Wagner, M. Hegner, P. Kernen, F. Zaugg, G. Semenza, "Covalent immobilization of native biomolecules onto Au(111) via N-hydroxysuccinimide ester functionalized self-assembled monolayers for scanning probe microscopy," *Biophys J* ***70***, pp. 2052-2066, 1996.
58. N. Patel, M. C. Davies, M. Hartshorne, R. J. Heaton, C. J. Roberts, S. J. B. Tendler, P. M. Williams, "Immobilization of protein molecules onto homogeneous and mixed carboxylate-terminated self-assembled monolayers," *Langmuir* ***13***, pp. 6485-6490, 1997.
59. K. Wadu-Mesthrige, N. A. Amro, G.-Y. Liu, "Immobilization of Proteins on Self-Assembled Monolayers," *Scanning* ***22***, pp. 380-388, 2000.
60. K. Wadu-Mesthrige, N. A. Amro, J. C. Garno, S. Xu, G.-Y. Liu, "Fabrication of Nanometer-Sized Protein Patterns Using Atomic Force Microscopy and Selective Immobilization," *Biophys. J.* ***80***, pp. 1891-1899, 2001.
61. G. Y. Liu, N. A. Amro, "Positioning protein molecules on surfaces: A nanoengineering approach to supramolecular chemistry," *Proc. Natl. Acad. Sci. U. S. A.* ***99***, pp. 5165-5170, 2002.
62. T. Imoto, L. N. Johnson, A. C. T. North, D. C. Philips, J. A. Rupley, *Vertebrate Lysozymes*; Academic Press: New York, 1972; Vol. 7.
63. K. Hu, A. J. Bard, "Use of atomic force microscopy for the study of surface acid-base properties of carboxylic acid-terminated self-assembled monolayers," *Langmuir* ***13***, pp. 5114-5119, 1997.
64. C. F. Blake, D. F. Koenig, G. A. Mair, A. C. T. North, D. C. Phillips, V. R. Sarma, "Structure of Hen Egg-White Lysozyme," *Nature* ***206***, pp. 757-761, 1965.
65. K. Wadu-Mesthrige, N. A. Amro, J. C. Garno, S. Cruchon-Dupeyrat, G.-Y. Liu, "Contact Resonance Imaging-A Simple Approach to Improve the Resolution of AFM for Biological and Polymeric Materials," *Appl. Surf. Sci.* ***175-176***, pp. 391-398, 2001.
66. V. M. Rosenoer, M. Oratz, M. A. Rothschilde, *Albumin Structure and Function*; Pergamon Press: New York, 1977.
67. M. Liu, N. A. Amro, J. C. Garno, C. Chow, G.-Y. Liu, "Production of Nanostructures of DNA on Surfaces," *Nano Letters*, pp. In Press, 2002.
68. J. C. Garno, N. A. Amro, K. Wadu-Mesthrige, G.-Y. Liu, "Production of Periodic Arrays of Protein Nanostructures Using Particle Lithography," *Nano Letters*, pp. Submitted, 2002.